Applied Energy 256 (2019) 113926

Contents lists available at ScienceDirect

Applied Energy

journal homepage: www.elsevier.com/locate/apenergy

Optimal renewable generation and battery storage sizing and siting considering local transformer limits

Laura Novoa, Robert Flores*, Jack Brouwer

Advanced Power and Energy Program, University of California, Irvine, USA

HIGHLIGHTS

- An optimization for DER allocation incorporates utility transformer constraints.
- A polygon relaxation models the apparent power flow through power transformers.
- TOU, NEM, and wholesale rates are modeled for each utility customer type.
- A novel, renewable energy battery storage is modeled to export under NEM rates.

ARTICLE INFO

Keywords:
Distributed Energy Resource Optimization
Transformer constraints
Mixed integer linear program
Battery energy storage
Microgrid
Zero Net Energy

ABSTRACT

In response to climate change and sustainability challenges, various incentive programs have increased solar photovoltaic (PV) generation interconnection in the low voltage electrical distribution system. However, electric utility support of PV generation is limited by reverse power flow into the electricity network at high penetration levels. This limits the ability to achieve Zero Net Energy (ZNE) behind individual meters and in whole communities. In parallel, district level energy systems, and Advanced Energy Communities (AEC) that include storage, offer a great prospect for integrating high levels of Distributed Energy Resources (DER) into the built environment. Optimally designing such systems to serve communities, commercial, and industrial loads, while maximizing the penetration of solar PV, has been a challenge to Distribution System Operators (DSO) and city planners. This paper proposes a Mixed Integer Linear Program (MILP) optimization to decide the best DER portfolio, allocation, and dispatch, for an AEC that achieves ZNE and islanding while respecting electrical grid operational constraints, with a focus on distribution transformer overloads. The main strategies to avoid transformer overloads were found to be judicious sizing and siting of battery energy storage and also optimally re-distributing PV throughout the community, which increased the ability of the electric infrastructure to support a PV deployment that is 1.7 times larger than the existing transformer capacity without the need for infrastructure upgrades. This work highlights the importance of including local infrastructure capacities, such as distribution transformer constraints when developing projects that result in high renewable penetration throughout the distribution network.

1. Introduction

A significant challenge involving DER integration into the utility grid network is to allocate (*i.e.*, to assign an amount or portion of a resource) to a particular recipient node, which entails both sizing and siting these resources into the existing electric distribution grid. Ideally, DER allocation and dispatch can be done, so that no additional distribution infrastructure upgrade is required. Known issues caused by DER, specifically PV systems when installed in high-penetration, include but are not limited to voltage rise during low load periods, and reverse power flow, that is, a flow of power from a section of a radial circuit towards the main distribution substation, which increases electric power losses and creates issues in protection equipment [1,2]. Solving the problems mentioned above is essential to promote an increase in the PV hosting capacity of urban district systems, which are rising to be one of the most effective ways to integrate not only PV but a suite of DER into a local distribution grid. Thus, the types of DER, their allocation within the system, as well as their operation and dispatch have to be carefully chosen to improve the overall system performance while meeting customer demand. Judicious and systemic DER

* Corresponding author at: University California, Irvine, CA 92697, USA.
E-mail address: rjf@apep.uci.edu (R. Flores).

https://doi.org/10.1016/j.apenergy.2019.113926
Received 16 May 2019; Received in revised form 5 August 2019; Accepted 19 September 2019
Available online 10 October 2019
0306-2619/ © 2019 Elsevier Ltd. All rights reserved.

Nomenclature

AEC	Advanced Energy Community
C&I	Commercial and Industrial
DER	Distributed Energy Resource
DERopt	Distributed Energy Resource Optimization
DG	Distributed Generation
DSO	Distribution System Operator
EES	Electric Energy Storage
HC	Hosting Capacity
MILP	Mixed Integer Linear Program
MV/LV	Medium Voltage/Low Voltage
NEM	Net Energy Metering
O&M	Operation and Maintenance
PCC	Point of Common Coupling
PF	Power Factor
REES	Renewable Electric Energy Storage
TOU	Time-of-Use
ZNE	Zero Net Energy

deployment (allocation and dispatch) is recommended over random deployment [3] and is essential to enable the very high PV penetrations required for ZNE.

Simultaneously, there has been much recent interest in developing the concept of Advanced Energy Communities — electrically contiguous areas that leverage the clustering of load and generation by integrating multiple utility customer-owned DER [4]. Within an AEC, DER assets allow for most of the energy demand to be generated and consumed internally. External energy transfers enter the community if local production is insufficient. Excess electricity is exported to the wide-area electricity grid. AECs can operate grid-connected or as islanded microgrids (for resiliency purposes) under certain circumstances of containing a sufficient DER to match the loads and a microgrid controller, AECs and microgrids may share typical DER and local control resources and electric infrastructure topology. Moreover, AECs facilitate the integration of clean and innovative DER technologies into the existing utility grid infrastructure, minimizing the need for upgrades while maximizing the local renewable generation hosting capacity to provide environmental, societal, and utility benefits [4].

The present work evaluates a piece of the broader AEC vision, assuming total electrification of community energy demand as ZNE developments are expected to be introduced [5]. Moreover, we only consider PV and battery storage as our DER. Nonetheless, the analysis and models developed can be easily extended to include a broader variety of DER, such as hydrogen energy storage or renewable fueled fuel cell systems.

For most AECs, the ultimate goal is to allow for ZNE operation. To achieve ZNE operation, a big challenge is how to increase the hosting capacity (HC), *i.e.,* the maximum DER penetration for which the power system infrastructure operates satisfactorily [6], in urban distribution systems. Historically, DSOs have employed rules-of-thumb for DER integration. The “15% rule” only allows for DER penetration below 15% of the local maximum load [7]. Various other DSOs have employed (and some still employ) similar rules of thumb. For example, in Canada, DG deployment shouldn’t exceed 60% of the transformer rating at the main substation. In Portugal, the total DG ratings should be lower than 25% of the medium voltage/low voltage (MV/LV) transformer rating. In Spain, the total DG ratings should be lower than 50% of the MV/LV transformer rating and lower than 50% of the thermal limit of the affected feeders. In Italy, the total DG ratings should be lower than 65% of the MV/LV transformer rating and lower than 60% of the thermal limit of the affected feeders [8]. These conservative and somewhat arbitrary rules are practical but impose a limit to achieving high-penetration of renewable generation and ZNE.

On the other hand, increasing HC could provide more realistic and accurate results. In California, DSOs have been required to provide a high-level HC analysis of their medium voltage circuits with some utilities developing interactive GIS map tools, such as DERiM maps [9]. However, the DER allocation in the lower voltage (< 12 kV) portion of the circuit, specifically regarding distribution transformer constraints, has not been addressed.

Given the need of deploying PV in high penetrations to meet AEC ZNE goals, a significant share of AEC project success depends upon achieving an adequate allocation of DER such as PV and battery storage resources while supporting and enhancing the overall utility grid network characteristics. There have been numerous state-of-the-art optimization approaches applied to the development of computational tools for the investment planning and operation of DER. In district systems, DER allocation can be performed optimally to maximize benefits to the utilities, project owners, and customers. These benefits include, but are not limited to: minimizing project cost, minimizing power system electric losses, maximizing renewable penetration, minimizing carbon emissions, maximizing the PV hosting capacity, or achieving zero-net-energy operation.

The underlying DER allocation problem is typically non-linear, highly constrained, multi-objective, mixed-integer, and multi-modal. Thus, finding a global-optimal solution is challenging [10]. Known optimization techniques used in the literature include, but are not limited to linear programming (LP), mixed integer linear programming, mixed integer non-linear programming (MINLP), dynamic programming (DP), sequential quadratic programming (SQP), ordinal optimization (OO), cone programming (CP), and heuristic methods such as genetic algorithms (GA) and particle swarm optimization (PSO) [11].

Amongst the most common approaches are MILP formulations, in which only some variables are constrained to be integers, while other variables are allowed to be continuous. Integer programs can model many practical situations, such as scheduling, and resource allocation [12] due to their flexibility in modeling constraints involving binary or integer decisions (yes or no, and on or off behaviors) There is also a wide availability of robust commercial solvers, that allow control and awareness of the optimality gap between optimal and integer solution [13]. MILP algorithms can be solved in polynomial time, that is, computing time is defined by a polynomial function of the instance size, therefore, the MILP computational burden increases significantly with the scale of the problem, typically requiring the program developer to balance model complexity with tractability [13].

The most straightforward DER allocation problem involves allocating a single specific type of DER at a single node, according to a particular optimization goal and a set of constraints. This analysis is usually performed by aggregating all loads and generation together (*i.e.*, “aggregate approach”) and assuming lossless transfer of energy between nodes. A number of enhancements to this approach were developed in subsequent literature, such as (1) optimizing a portfolio (mix) of DER [14], (2) considering the time-coupling of generation and load in a time-domain, dynamic simulation [15–19] (3) siting DER on different nodes of a network [20], (4) incorporating electricity grid constraints [21–25], (6) energy storage [26], (5) DER uncertainty [27,28], and (7) smart-grid technologies [29,30].

1.1. Related work

Many dynamic optimization approaches for DER allocation already exist where the objective function is to allocate DER and also dispatch DER such that cost is minimized, or other multi-objective formulation. A few examples of such analyses are presented below.

Falke et al. [17] developed a multi-objective optimization for the

design of a district electricity and heat supply system to minimize annual costs (investment, demand, and operation) of energy supply and CO_2 emission equivalents. The decision variables included the heating network connections, DER types, sizes, and operation. The problem was decomposed into three subproblems (heating network, DER, and energy efficiency measures design, and DER operation) and solved iteratively to reduce computational complexity. The solution approach involved the heuristic spanning tree method (Kruskal's method), an evolutionary algorithm, and a deterministic operation simulation.

Flores et al. [31] developed a MILP model to minimize the cost of energy while limiting greenhouse gas (GHG) emissions. The decision variables used were DER type, size, and operation. Two primary technology scenarios were explored (DER including storage with and without electrical export). Li et al. [32] decomposed the DER allocation problem into leader-follower problem. The leader problem was a genetic algorithm to search for the best sizing values of each component to minimize cost. Each candidate solution was then fed into the follower problem, a MILP, which was used to solve the DER sizing and obtain the optimal energy management strategy.

In many publications that use these optimization strategies, authors did not include grid constraints (voltage at nodal buses, power flows through distribution lines and transformers), and assumed that the grid infrastructure has an unlimited capacity. Results from these studies are optimal for a distributed energy system comprised of a single node but may lead to suboptimality or infeasibility when applied to a distribution grid network [33]. Moreover, single-node, aggregate modeling approaches do not allow for DER siting and can under-estimate DER capacities and project costs, since they do not account for the electrical distribution grid infrastructure and its constraints and internal losses [33]. All previously mentioned literature sources do not include simultaneous optimization of (1) DER size and location, (2) DER operation, and (3) impact on the local power system infrastructure. Four recent studies; however, were found to address these sub-problems simultaneously.

Mashayekh et al. [24] used a MILP approach to determine optimal technology mix, size, placement, and dispatch in a multi-energy (electric, heating, and cooling) microgrid, using a multi-node, time-series approach. The objective (minimize cost or CO_2 emissions) was constrained by linearized power flow (LinDistFlow) constraints, nodal voltage constraints, and linearized apparent power constraints for cable current limits. The DER simulated in this study were P-type (can only output active power), but the building loads were assumed to consume reactive power at a fixed power factor. An 18-node radial test system was used as a case study, where DER was limited to be installed only at three pre-defined nodes within the network.

Another study was presented by Morjav et al. [21] which described a framework for computing optimal DER size, location, and type, in an energy hub. Different combinations of a genetic algorithm and a MILP were compared. For the MILP formulation, the objective of minimizing cost and CO_2 emissions was constrained by linearized Alternating Current (AC) power flow equalities, voltage limits ($\pm$ 10%), and linearized current limits using a combination of linearization techniques including a first-order Taylor series approximation, and piece-wise linearization of the squared real and imaginary current components. The test case consists of 5 residential buildings connected on a radial network. The authors noted that a system with more buildings would be computationally intractable.

Additional recent work by Ehsan et al. [34] proposed a Mixed Integer Quadratically Constrained program for the optimal DER mix, siting, and sizing in multi-energy microgrids considering load and generation uncertainties. The objective of minimizing cost and carbon emissions is constrained by the simplified non-linear DistFlow formulation of voltage and line apparent power flow limits. The DER is PQ (active and reactive power) type, but with no S (apparent power) limit coupling of P and Q. The test case used was a 19-bus radial microgrid.

Lastly, a recent study by Alturki et al. [35] developed an optimization-based hosting capacity calculation using MILP for sizing and siting DG aiming to maximize the total DG deployments. Voltage limits were constrained as well as DG output and line capacities considering active and reactive power flows separately (*i.e.*, without considering the apparent power coupling). The IEEE-33 bus radial distribution grid was used as a test case. The near-optimal HC solution calculated by this method was found superior compared to traditional iterative HC calculation methods. While this study presented a brilliant strategy for maximizing PV penetration, the active and reactive power flow coupling was not captured.

The survey of current literature shows that the focus on modern multi-nodal DER allocation methods has been on ensuring feasible power flow between nodes while maintaining acceptable voltage levels. These previous approaches typically do not include:

- Limiting the power flow injections through distribution transformers; recent projects on large scale urban district systems [36] suggest that transformer overloads will be a significant hurdle for DER integration into the urban low voltage network.
- The coupling between active (P) and reactive (Q) power in power flow constraints, due to its non-linear relationship ($S = \sqrt{P^2 + Q^2}$)
- Large-scale test cases. Current formulations typically use a large number of constraints involving binary and integer variables, which can make the problem computationally intractable. Hence, most test-cases in the literature consider only small and non-scalable grid networks.
- The variety of utility electricity tariffs that a mix of residential and commercial and industrial (C&I) utility customers are subjected to, and the different markets where renewable DER can participate, namely Net-Energy-Metering (NEM) and wholesale.
- Explicit models of battery storage systems that can only charge from renewable sources, and in turn, meet utility requirements for exporting under NEM rates.
- The limited physical area available for a realistic DER deployment into the built urban environment.

1.2. Contributions of the current work

This study proposes a mixed integer linear program optimization to allocate PV and battery storage size and location across an AEC with complex existing distribution grid infrastructure. The objective is to minimize cost throughout the time-resolved dynamic operation of the system during a representative year using known load and solar insolation profiles. Desired operation goals such as Zero-Net-Energy and islanding as a microgrid for resiliency during unplanned grid outages are also modeled. The electrical distribution network is modeled in a multi-nodal approach, and the flows of both active and reactive power are taken into account. For a realistic formulation of the DER allocation problem, minimum discretized DER sizes are enforced so that the global optimal solution can be guaranteed within a pre-defined optimality gap.

The present work adds to the previous literature by proposing a novel, yet straight-forward, approach to avoid distribution transformer overloads by constraining non-linear nodal apparent power injections with the use of polygon relaxations, which is less computationally intensive than piecewise-linearization since it does not need the addition of binary variables and special ordered sets.

In summary, the contributions of the current work are:

- The optimal DER allocation for a real-world electric distribution system, here defined as an Advanced Energy Community microgrid, considering its aggregated behavior as a grid-connected system or islanded, its diverse load profiles (residential, commercial and industrial) and limited physical space for DER deployment.
- Distribution transformer apparent (S) power flows are explicitly limited through a novel constraint, using a straightforward linearization method that allows for the test system to be scaled to more

than 30 nodes;
- Electricity rates used to account for the realistic time of use (TOU) and demand rate structures for each individual residential, commercial, or industrial customer. Also, DER is allowed to take advantage of different market mechanisms such as NEM and wholesale rates, to add revenue streams;
- A novel storage concept is modeled, namely the Renewable-tied Energy Storage System (REES) *i.e.*, storage that charges exclusively from renewable solar PV energy, which is for that reason allowed to export electricity back to the utility grid under NEM rates; and
- District or community-wide operation goals such as Zero Net Energy and islanding are modeled.

2. Problem formulation

The optimization formulation presented here builds upon the work presented in Flores et al. [18,31], namely the DERopt tool. We review the original problem formulation in Sections 2.2 and 2.3 and expand upon the prior by introducing reactive power balances to the original formulation and transformer constraints with a polygon relaxation method, presented in Section 2.4.

2.1. Model sets, parameters, and decision variables

The applicable sets for the optimization model are:

- $n \in \mathrm{N}$: Set of all months
- $t \in \mathrm{T}_n$: Set of all hourly increments in month n
- $m \in \mathrm{M}$: Set of all summer months ($\mathrm{M} \subset \mathrm{N}$)
- $o \in \mathrm{O}_m$: Set of all hourly increments during on-peak in summer month m ($\mathrm{O} \subset \mathrm{T}$)
- $p \in \mathrm{P}_m$: Set of all hourly increments during mid-peak in summer month m ($\mathrm{P} \subset \mathrm{T}$)
- $b \in \mathrm{B}$: Set of all buildings
- $x \in \mathrm{X}$: Set of all transformers
- $j \in \mathrm{J}_x$: Set of buildings that are connected to transformer $\times$ ($\mathrm{J} \subset \mathrm{B}$)
- $\lambda \in \Lambda$: Set of line segments for polygon relaxation

The applicable decision variables and parameters for the optimization model can be seen in Table 1 and Table 2, respectively.

2.2. Objective function

The objective function is the sum of various individual cost components to be minimized. The cost parameters, defined by the Cvariables, include the cost of utility grid imports ($\mathrm{C_{grid}}$), demand charges (C_{DC}, $C^{\mathrm{on}}_{\mathrm{DC}}$, $C^{\mathrm{mid}}_{\mathrm{DC}}$), the cost to purchase ($\mathrm{C_{cap}}$) and operate DER ($\mathrm{C_{O\&M}}$), and the revenue generated by exporting excess electricity to the grid under both NEM ($\mathrm{C_{NEM}}$) and wholesale rates ($\mathrm{C_W}$). The cost parameters are multiplied by the specific decision variables, which include the building hourly power flows (P variables for import, PV production, and battery charge and discharge), the maximum power demand over a month ($\mathrm{P_{DC}}$ variables), and the PV/EES/REES capacity adopted (S_{PV}, S_{EES} and S_{REES}). All individual cost components are added through a specific time interval: t (hourly), n (monthly), or m (during summer months), and across all buildings b as follows in Eq. (1). Therefore, the first line of the objective function captures the costs associated with purchase and sale of energy, the second line captures the cost associated with demand charges, and the third, fourth and fifth lines capture the cost associated with purchasing and operating the adopted DER.

$$\begin{aligned}\text{minimize}\quad & \sum_{b=1}^{B}\Big(\sum_{t=1}^{T} C_{\mathrm{grid}_{t,b}} P_{\mathrm{import}_{t,b}} - C_{\mathrm{NEM}_{t,b}}\left(P_{\mathrm{PV_{NEM},t,b}} + P_{\mathrm{REES_{NEM},t,b}}\right) \\ & - C_{W_t} P_{\mathrm{PV_{W},t,b}} + \sum_{n=1}^{N} C_{\mathrm{DC}_n} P_{\mathrm{DC}_{n,b}} \\ & + \sum_{m=1}^{M}\left(C^{on}_{\mathrm{DC}_m} P^{on}_{\mathrm{DC}_{m,b}}\right) + \sum_{m=1}^{M}\left(C^{mid}_{\mathrm{DC}_m} P^{mid}_{\mathrm{DC}_{m,b}}\right) \\ & + C^{\mathrm{PV}}_{\mathrm{cap}} S_{\mathrm{PV}_b} + C^{\mathrm{PV}}_{\mathrm{O\&M}}\left(P_{\mathrm{PV_{BLDG},t,b}} + P_{\mathrm{PV_{NEM},t,b}} + P_{\mathrm{PV}_{W,t,b}}\right) \\ & + C^{\mathrm{EES}}_{\mathrm{cap}} S_{\mathrm{EES}_b} + C^{\mathrm{EES}}_{\mathrm{O\&M}}\left(P_{\mathrm{EES_{ch},t,b}} + P_{\mathrm{EES_{dch},t,b}}\right) \\ & + C^{\mathrm{REES}}_{\mathrm{cap}} S_{\mathrm{REES}_b} + C^{\mathrm{REES}}_{\mathrm{O\&M}}\left(P_{\mathrm{REES_{ch},t,b}} + P_{\mathrm{REES_{dch},t,b}} + P_{\mathrm{REES_{NEM},t,b}}\right)\Big)\end{aligned} \tag{1}$$

The objective function is minimized subject to a set of equality and inequality constraints, and also integer constraints, which are detailed in the following sections.

2.3. General constraints

In this optimization formulation, equality and inequality constraints are formulated to:

- Ensure the electrical energy balance within each building, *i.e.*, the electrical demand of the building, is entirely met at each time step while maintaining feasible operation;
- Set maximum and minimum generation output constraints for each DER;
- Control the operation of all electrical energy storage systems; and
- Limit the states of charge and charging rates for each battery system.

A concept similar to the Energy Hub, introduced in Morvaj et al. [21], is explored here, but only applied to electricity balances. Here, each building and its connected DER (PV, EES, and REES) represent a Building Energy Hub. Hence, the electricity needs of every building are

Table 1
List of decision variables used in DERopt.

Decision Variable	Description	Units
$P_{\mathrm{import}_{t,b}}$	Power imported from the grid to building b at hour t	kW
$P_{\mathrm{DC}_{n,b}}$	Maximum demand during month n at building b	kW
$P^{\mathrm{on}}_{\mathrm{DC}_{m,b}}$, $P^{\mathrm{mid}}_{\mathrm{DC}_{m,b}}$	Maximum on-peak and mid-peak demand during summer month m and building b	kW
S_{PV_b}	Solar PV capacity adopted at building b	kW
$P_{\mathrm{PV_{BLDG},t,b}}$	Power generated by solar PV at hour t at building b	kW
$P_{\mathrm{PV_{NEM},t,b}}$	Power exported under NEM rates at hour t from building b	kW
$P_{PV_{W},t,b}$	Power exported under wholesale rates at hour t from building b	kW
S_{EES_b}, S_{REES_b}	EES/REES capacity adopted at building b	kWh
$e_{\mathrm{EES}_{t,b}}$, $e_{\mathrm{REES}_{t,b}}$	EES/REES state of charge t hour t at building b	kWh
$P_{\mathrm{EES_{ch},t,b}}$, $P_{\mathrm{REES_{ch},t,b}}$	EES/REES charging power at hour t at building b	kW
$P_{\mathrm{EES_{dch},t,b}}$, $P_{\mathrm{REES_{dch},t,b}}$	EES/REES discharging power at hour t at building b	kW
$P_{\mathrm{REES_{NEM},t,b}}$	Power exported from REES at NEM rates at hour t at building b	kW
n_{EES}, n_{REES}	Binary variable indicating EES/REES adoption at building b	n/a
P_{T_x}, Q_{T_x}, S_{T_x}	Active, Reactive, and Apparent Power flows through transformer x at hour t	kW/kVAr/kVA

Table 2
List of parameters used in DEROpt.

Parameter	Description	Units	Value
$P_{\mathrm{BLDG}_{t,b}}$, $Q_{\mathrm{BLDG}_{t,b}}$	Power (active and reactive) demand at building b, at hour t	kW/kVAr	Based on URBANopt outputs
A_b	Area available for solar PV installation at building b	m^2	Based on methods described in Section
I_t	Normalized Average available insolation at hour t	kW/kWp	Taken from [37]
$C_{\mathrm{grid}_{t,b}}$	Utility electricity charge at hour t at building b	$/kWh	Southern California Edison Rate Structures
$C_{\mathrm{DC}n}$	Non-TOU demand charge in month n	$/kW	14.88
$C_{\mathrm{DC}m}^{\mathrm{on}}$, $C_{\mathrm{DC}m}^{\mathrm{mid}}$	On-peak and Mid-peak demand charge in summer month m	$/kW	23.74 (on) 6.55 (mid)
$C_{\mathrm{NEM}_{t,b}}$	Net energy metering price at which electrical utility purchases energy from building b at hour t	$/kWh	Energy charge $C_{\mathrm{grid,t}}$ minus transmission and distribution cost
$C_{\mathrm{W}_{t,b}}$	Wholesale price at which electrical utility purchases energy from building b at hour t	$/kWh	0.03
C_{Cap}^{PV}	Capital cost for solar PV system	$/kW	2000
$C_{\mathrm{O\&M}}^{PV}$	O&M cost for solar PV system	$/kWh	0.001
η_{PV}	Efficiency of PV at nominal conditions	%	18
$C_{\mathrm{Cap}}^{\mathrm{EES}}$, $C_{\mathrm{Cap}}^{\mathrm{REES}}$	Capital cost of EES/REES	$/kWh	600
$C_{\mathrm{O\&M}}^{\mathrm{EES}}$, $C_{\mathrm{O\&M}}^{\mathrm{REES}}$	Cost to charge/discharge EES/REES	$/kWh	0.001[18]
α	Retained EES/REES storage between hourly periods	%	99.99
$\eta_{\mathrm{EES_{ch}}}$ $\eta_{\mathrm{EES_{dch}}}$	EES/REES charging efficiency	%	90
$\eta_{\mathrm{REES_{ch}}}$, $\eta_{\mathrm{REES_{dch}}}$	EES/REES charging efficiency	%	90
$\bar{\delta}_{\mathrm{EES}}$, $\bar{\delta}_{\mathrm{REES}}$	Maximum EES/REES state of charge	% of purchased capacity	95
$\underline{\delta}_{\mathrm{EES}}$, $\underline{\delta}_{\mathrm{REES}}$	Minimum EES/ REES state of charge	% of purchased capacity	10
$\bar{\mu}_{\mathrm{EES}}$, $\bar{\mu}_{\mathrm{REES}}$	Maximum EES/ REES charging rate	% of purchased capacity	25
$\underline{\mu}_{\mathrm{EES}}$, $\underline{\mu}_{\mathrm{REES}}$	Maximum EES/ REES discharging rate	%of purchased capacity	25
$\bar{S}_{\mathrm{EES}}$, $\bar{S}_{\mathrm{REES}}$	Big M constant for EES/REES size	kWh	99,999
$\underline{S}_{\mathrm{EES}}$, $\underline{S}_{\mathrm{REES}}$	Minimum EES/REES size	kWh	13.5
$\bar{S}_{\mathrm{Tx}}$	Power Rating of transformer x	kVA	Based on power system topology
PF	Building power factor	n/a	0.90 (Residential) 0.85 (C&I)
α_x	Transformer x p.u. loading	%	1
σ_b	Max PV installation coefficient at building b	kW/ft^2	0.005 (Residential) 0.009 (C&I)
θ_λ	Angle of segment λ of polygon relaxation	degrees	Based on the number of polygon sidesΛ
Λ	Number of sides for polygon relaxation	n/a	22

to be met by an optimally sized combination of PV, EES, REES, and electricity imports. The model also makes the distinction between active (P), reactive (Q), and apparent (S) power flows. Considering active power, Eq. (2) requires that at all times t, for every building b, the active electrical load ($P_{\mathrm{BLDG}_{t,b}}$) plus any EES charging ($P_{\mathrm{EES_{ch}}t,b}$), is met through electricity imports ($P_{\mathrm{import}_{t,b}}$), currently available solar production sent to the building ($P_{\mathrm{PV_{BLDG},t,b}}$), and the discharging of any EES or REES assets ($P_{\mathrm{EES_{dch,t,b}}}$ and $P_{\mathrm{REES_{dch,t,b}}}$). Considering reactive power, Eq. (3) requires that, the reactive electrical load of each building ($Q_{\mathrm{BLDG}_{t,b}}$), which will depend upon a fixed local power factor (PF) will be entirely met by utility reactive power imports ($Q_{\mathrm{import}_{t,b}}$). Note that no security or reliability margins are included in our formulation.

$$P_{\mathrm{import}_{t,b}} + P_{\mathrm{PV_{BLDG},t,b}} + P_{\mathrm{EES_{dch},t,b}} + P_{\mathrm{REES_{dch},t,b}} = P_{\mathrm{BLDG}_{t,b}} + P_{\mathrm{EES_{ch},t,b}} \quad (2)$$

$$Q_{\mathrm{import}_{t,b}} = Q_{\mathrm{BLDG}_{t,b}} = \mathrm{P_{BLDG}}\arctan(PF) \quad (3)$$

Eqs. (4)–(6) relate electrical imports to both non-TOU and TOU demand charges. Where subscripts o and p are the set of all hourly increments during on-peak and mid-peak, respectively, in summer month m.

$$P_{\mathrm{import_{t,b}}} \leq P_{DC_{n,b}} \quad (4)$$

$$P_{\mathrm{import_{o,b}}} \leq P_{\mathrm{DC}_{m,b}}^{\mathrm{on}} \quad (5)$$

$$P_{\mathrm{import_{p,b}}} \leq P_{\mathrm{DC}_{m,b}}^{\mathrm{mid}} \quad (6)$$

Solar PV adoption and operation constraints are shown in Eqs. (7) and (8). Eq. (7) limits PV production by the PV capacity adopted (S_{PV_b}) and available insolation (I_t). Eq. (8) limits the size of the PV adoption at each building according to the maximum available rooftop area (A_b) and the kW/ft^2 ratio (σ).

$$P_{\mathrm{PV_{BLDG},t,b}} + P_{\mathrm{PV_{NEM},t,b}} + P_{\mathrm{PV}_{W,t,b}} + P_{\mathrm{REES_{ch},t,b}} \leq I_t S_{\mathrm{PV}_b} \quad (7)$$

$$S_{\mathrm{PV}_b} \leq \sigma A_b \quad (8)$$

Within electrical energy storage, the model considers two types of storage, (1) electrical energy storage, or EES, which can store imported utility electricity and excess renewable produced onsite and also (2) renewable electric energy storage, or REES, which is the storage exclusively supplied by renewable onsite PV. A distinction between EES and RESS is made because only energy storage exclusively charged using renewable energy is allowed to be exported to the grid under California NEM rates. Both the EES and REES share similar types of constraints. Eqs. (9) and (13) show the energy balance for the EES and REES respectively. The difference between EES and REES is the presence of the $P_{REES_{NEM,t,b}}$ variable, allowing electricity export from any adopted REES. Note that wholesale import, *i.e.,* electricity imported to the building, billed at wholesale prices, is not considered for REES charging since initial simulations indicated that this pathway is not economically attractive due to the REES round trip efficiency. Eqs. (10) and (14) limit the maximum state of charge by the installed capacity for the EES and REES, respectively. Eqs. (11) and (15) limit the maximum discharge rate by the size of the adopted battery, and Eqs. (12) and (16) limit charging to the battery for the EES and REES system, respectively. Eqs. (17) and (18) require that if EES and REES systems are adopted, a minimum system size is installed. Minimum battery size is based upon the popular Tesla Powerwall size of 13.5 kWh [38]. The variables n_{EES_b} and n_{REES_b} are binary variables, that is, integer variables that are restricted to values of 0 or 1.

$$e_{\mathrm{EES}_{t,b}} = \alpha_{\mathrm{EES}} e_{\mathrm{EES}_{(t-1),b}} + \eta_{\mathrm{EES}_{\mathrm{ch}}} P_{\mathrm{EES}_{\mathrm{ch},t,b}} - \frac{P_{\mathrm{EES}_{\mathrm{dch},t,b}}}{\eta_{\mathrm{EES}_{\mathrm{dch}}}} \tag{9}$$

$$\underline{\delta}_{\mathrm{EES}} E_{\mathrm{EES}_b} \leq e_{\mathrm{EES}_{t,b}} \leq \bar{\delta}_{\mathrm{EES}} E_{\mathrm{EES}_b} \tag{10}$$

$$P_{\mathrm{EES}_{\mathrm{dch},t,b}} \leq \bar{\mu}_{\mathrm{EES}} S_{\mathrm{EES}_b} \tag{11}$$

$$P_{\mathrm{EES}_{\mathrm{ch},t,b}} \leq \underline{\mu}_{\mathrm{EES}} S_{\mathrm{EES}_b} \tag{12}$$

$$e_{\mathrm{REES}_{t,b}} = \alpha_{\mathrm{REES}} e_{\mathrm{REES}_{(t-1),b}} + \eta_{\mathrm{REES}_{\mathrm{ch}}} P_{\mathrm{REES}_{\mathrm{ch},t,b}} - \frac{P_{\mathrm{REES}_{\mathrm{dch},t,b}} + P_{\mathrm{REES}_{\mathrm{NEM},t,b}}}{\eta_{\mathrm{EES}_{\mathrm{dch}}}} \tag{13}$$

$$\underline{\delta}_{\mathrm{REES}} E_{\mathrm{REES}_b} \leq e_{\mathrm{REES}_{t,b}} \leq \bar{\delta}_{\mathrm{REES}} E_{\mathrm{REES}_b} \tag{14}$$

$$P_{\mathrm{REES}_{\mathrm{dch},t,b}} + P_{\mathrm{REES}_{\mathrm{NEM},t,b}} \leq \bar{\mu}_{\mathrm{REES}} S_{\mathrm{REES}_b} \tag{15}$$

$$P_{\mathrm{REES}_{\mathrm{ch}t,b}} \leq \underline{\mu}_{\mathrm{REES}} S_{\mathrm{REES}_b} \tag{16}$$

$$(1 - n_{\mathrm{EES}_b}) \underline{S}_{\mathrm{EES}} \leq S_{\mathrm{EES}_b} \leq (1 - n_{\mathrm{EES}_b}) \bar{S}_{\mathrm{EES}} \tag{17}$$

$$(1 - n_{\mathrm{REES}_b}) \underline{S}_{\mathrm{REES}} \leq S_{\mathrm{REES}_b} \leq (1 - n_{\mathrm{REES}_b}) \bar{S}_{\mathrm{REES}} \tag{18}$$

Eq. (19) constrains the value of exported electricity under NEM rates to the cost of imported electricity. Eq. (20) imposes the ZNE operation, *i.e.*, total imports must be less than or equal to total exports by the end of the year.

$$\sum_{b=1}^{B} \sum_{t=1}^{T} C_{\mathrm{NEM}_{t,b}} (P_{\mathrm{PV}_{\mathrm{NEM},t,b}} + P_{\mathrm{REES}_{\mathrm{NEM},t,b}}) \leq \sum_{b=1}^{B} \sum_{t=1}^{T} C_{\mathrm{grid}_{t,b}} P_{\mathrm{import}_{t,b}} \tag{19}$$

$$\sum_{b=1}^{B} \sum_{t=1}^{T} P_{\mathrm{PV}_{\mathrm{NEM},t,b}} + P_{\mathrm{PV}_{\mathrm{W,t,b}}} + P_{\mathrm{REES}_{\mathrm{NEM},t,b}} \leq \sum_{b=1}^{B} \sum_{t=1}^{T} P_{\mathrm{import}_{t,b}} \tag{20}$$

2.4. Transformer constraints and polygon relaxation

Here, we extend the formulation to a multi-node approach, where every Building Energy Hub (*i.e.*, building load and corresponding DER resources) is connected to spatially resolved nodes instead of a single physical (aggregated) node. The multi-node method allows for the modeling of the electric power distribution grid and the constraints involved with the physical power network and equipment.

The maximum amount of current limits the power capacity of a transformer at the rated voltage without exceeding the design temperature. Ratings are specified in kilovolt-amperes (kVA), which corresponds to the total apparent power that can flow through transformer windings, which includes active (kW) and reactive (kVAr) power flows [39], as shown in Fig. 2. Transformer overloads are typically acceptable for a short amount of time, and a typical transformer loading curve varies according to different ambient temperatures [40]. Nonetheless, even short periodic overload conditions will affect the equipment lifespan and maintenance needs.

We assume a distribution transformer is connected to a given node in the network and serves one or a cluster of Building Energy Hubs. Fig. 1 illustrates one such transformer T_x, which supplies only one Building Energy Hub, and its associated Solar PV and battery electric energy storage systems.

As shown in Fig. 1, each building has a net energy flow of imports minus exports from solar PV and REES. The net real and reactive power flows for all building energy hubs that are connected to the same transformer are aggregated, for each time step t (not explicit), using Eqs. (21) and (22).

$$P_{\mathrm{T}_x} = \sum_{j \in J_k} P_{\mathrm{import}_j} - P_{\mathrm{PV}_{\mathit{NEM},j}} - P_{\mathrm{PVW,j}} - P_{\mathrm{REES}_{\mathrm{NEM,j}}} \tag{21}$$

$$Q_{\mathrm{T}_x} = \sum_{j \in J_k} Q_{\mathrm{import}_j} \tag{22}$$

In Eqs. (23) and (24), for each time step, the apparent power flowing through a given transformer x, S_{Tx}, defined by the vectorial sum of active and reactive power, cannot exceed a given percentage (α) of its kVA rating ($\bar{S}_{T_x}$), where α is a coefficient used to allow under and overloading. Ultimately, all buildings and DER will have a transformer, or node, with such constraints associated with it.

$$S_{\mathrm{T}_x} = \sqrt{P_{\mathrm{T}_x}^2 + Q_{\mathrm{T}_x}^2} \tag{23}$$

$$S_{\mathrm{T}_x} = \alpha \bar{S}_{\mathrm{T}x} \tag{24}$$

Since a MILP method cannot directly capture the nonlinear constraints shown in Eqs. (23) and (24), a polygon relaxation of the

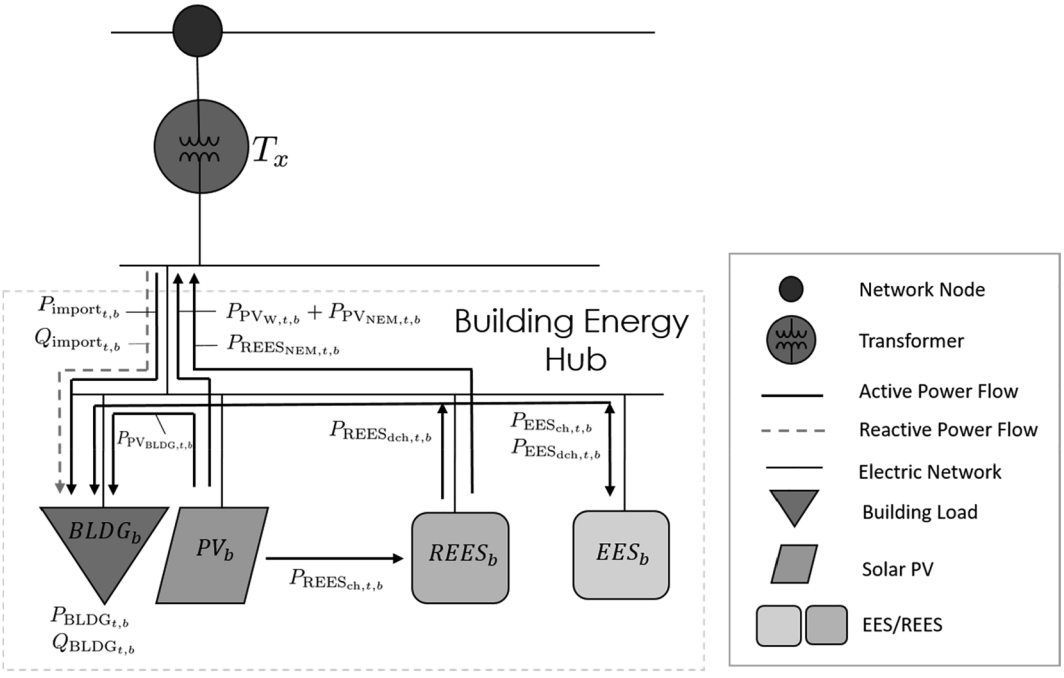

Fig. 1. Schematic of one Building Energy Hub used in the multi-nodal approach. Transformer T_x is one node, to which a cluster of buildings and DER are connected.

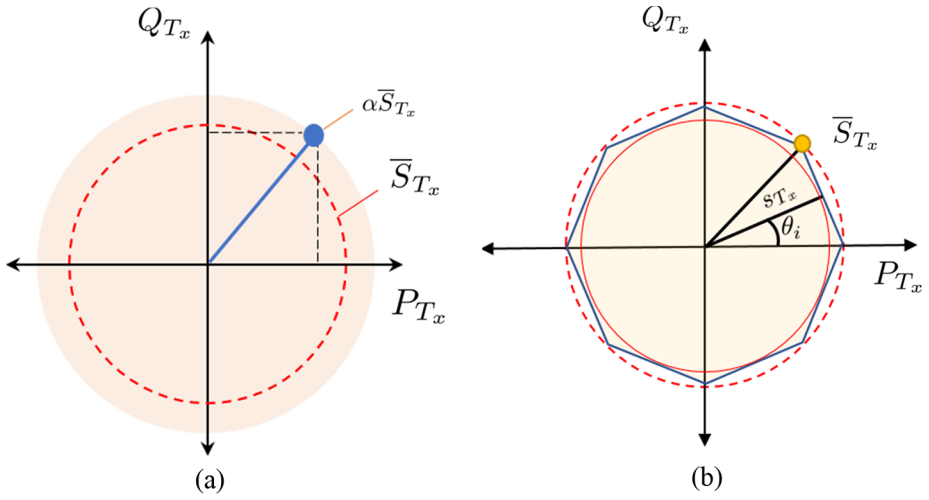

Fig. 2. (a) Operating regions for the transformer must be constrained so that $\alpha S_{T_x} = \sqrt{P_{T_x}^2 + Q_{T_x}^2}$ and (b) Depiction of the polygon relaxation constraint.

apparent power circle shown in Fig. 2 is performed. The method was inspired by Archimedes' π calculation process using polygons of an increased number of edges to approximate a circle [41]. This particular approach was used as an effective method for modeling directional thrust for a ship [42]. First, a polygon with Λ sides is inscribed inside the circle created by Eq. (23). A second circle with radius $s_{T_x} < \bar{S}_{T_x}$ can be inscribed within the polygon. In this case, the maximum s_{T_x} is defined by $s_{T_x} = \bar{S}_{T_x}\cos\left(\frac{\pi}{\Lambda}\right)$, where increasing the number of sides Λ decreases the difference between maximum s_{T_x} and $\bar{S}_{T_x}$. Considering that the error as defined by the difference between s_{T_x} and $\bar{S}_{T_x}$ is given by Eq. (25), absolute error can be reduced below 1% by setting the number of polygon sides Λ to 22. Using this approximation, power through a transformer can be written as Eq. (26), and implemented directly into the MILP optimization model as Eq. (27).

$$\epsilon = \bar{S}_{T_x} - s_{T_x} = \bar{S}_{T_x}\left(1 - \cos\frac{\pi}{\Lambda}\right) \rightarrow \Lambda \geq \frac{\pi}{\arccos\left(1 - \frac{\epsilon}{\bar{S}_{T_x}}\right)} \tag{25}$$

$$s_{T_x} = P_{T_x}\cos(\theta_\lambda) + Q_{T_x}\sin(\theta_\lambda),$$
$$\theta_\lambda = \frac{\pi}{\Lambda} + \lambda\left(\frac{2\pi}{\Lambda}\right),\ \lambda = 0, 1, \cdots, \Lambda - 1 \tag{26}$$

$$s_{T_x} \geq [\cos(\theta_\lambda)\ \sin(\theta_\lambda)]\begin{bmatrix} P_{T_x} \\ Q_{T_x} \end{bmatrix} \tag{27}$$

Similar polygon relaxation techniques have been explored and used in recent literature [24,43,44], but to the best of our knowledge, this concept has not been previously applied to limit transformer apparent power flows in a linear optimization.

3. AEC test case

The AEC design area encompasses a neighborhood in Huntington Beach, CA known as Oak View. The Oak View community includes over 300 buildings, including commercial and industrial operations, a primary school and library, and over 280 primarily multifamily homes. Full details of both demand and infrastructure modeling are presented in Brouwer et al. [36]. A summary of both modeling and the description of assumed DER properties used in the current work are presented in this section.

3.1. Electrical demand and resource modeling

Representative loads from the entire Oak View community building stock were selected from each of the three primary building sectors, namely, residential, commercial, and industrial. Detailed models of these buildings were developed in EnergyPlus [45]. The outputs of these building models were used as inputs to the current DERopt optimization. Examples of a residential, commercial, and year-round industrial demand, colored by season, are presented in Fig. 3.

The building energy simulations produced hourly-resolved loads over an entire year. In order to pursue a tractable optimization model, the building annual energy datasets are reduced using the k-medoids methodology presented in Domíngues et al. [46]. The building energy simulation data was filtered to yield three representative days for each

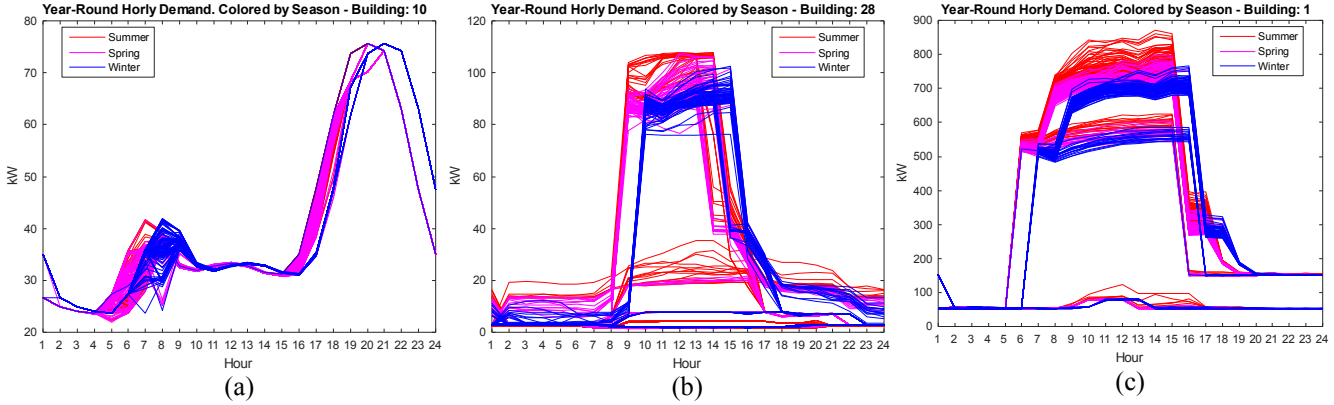

Fig. 3. URBANopt transformer-aggregated demand profiles for (a) Residential loads, (b) Commercial loads, and (c) Industrial loads. Color shows representative load variations for different seasons.

month. Finally, buildings behind a single transformer that are not subject to a demand charge were aggregated to reduce problem scale. Since the applicable Southern California Edison residential rates do not include a demand charge [47], most residential buildings were aggregated behind a single transformer. Thus, for residential loads, the terminology used here as "Building #" in fact refers to a cluster of residential buildings behind a single transformer.

Solar generation measured from a PV system installed at the University of California, Irvine was used as input [37]. The annual generation profile dataset captures and seasonal and weather variations.

Maximum PV capacity for each building (or group of residential buildings) was determined using aerial images of the neighborhood and the PV software HelioScope [48]. The maximum amount of PV kWp (kilowatts peak) that each rooftop in the Oak View community would be able to accommodate was determined considering rooftop geometry, set-backs and keep-outs determined by rooftop equipment, exhaust ports, and fire safety code requirements. From this survey, the kWp installed/ft^2 coefficient (σ)was determined to be 0.009 kWp installed/ft^2 for commercial and industrial buildings and 0.005 a kWp installed/ft^2 for residential buildings. A detailed list of all building load maximum demand, total energy demand, allowable PV area, in ft^2, the associated transformer number and its power rating, and building power factor is presented in Table 3.

Note that, in the Oak View case, the commercial and industrial rooftop area that is structurally capable of solar PV installation is relatively small in comparison to the loads in those same buildings. As a result, approximately 25% of some large industrial loads can be met through onsite solar PV. Prior to optimization, it is clear that community-scale ZNE in this particular community is only feasible when the remaining 75% is produced elsewhere in the community. Fig. 4 illustrates results from this analysis, where C&I buildings 3, 5, and 6 cannot meet their total annual energy demand with their own total annual onsite PV generation.

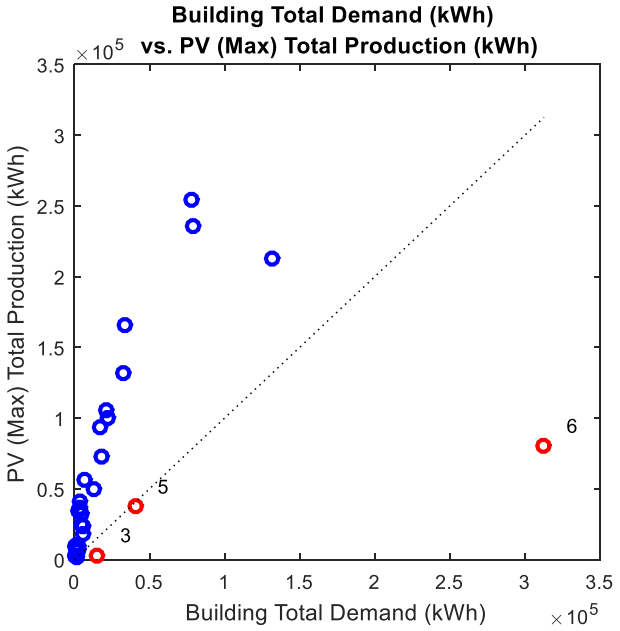

Fig. 4. Building total annual demand versus maximum total onsite yearly PV production, both in (kWh).

3.2. Electrical distribution infrastructure

An AEC microgrid test system (model) was developed based upon the real-world infrastructure installed in the Oak View neighborhood. The topology of the electrical power system is shown in Fig. 5. The Oak View AEC comprises single and multi-family residential buildings, a primary school, a library, a small park, and some industrial and

Table 3
AEC building loads, Maximum demand (kW), Total annual demand (kWh), Type, Rate Structure, Total Area (ft^2), Maximum rooftop PV installed (kW), Connected Transformer number, Transformer rating (kVA).

Building #	Max Load (kW)	Total (kWh)	Load Type	TOTAL Area (ft^2)	Max PV (kW)	PF	Transformer #	Transformer Rating (kVA)
1	872	2,743,640	I	140,086	1,296	0.8	37	1,250
2	27	78,338	I	23,843	221	0.8	40	37.5
3	100	327,587	I	1,892	18	0.8	28	150
4	18	57,404	I	22,673	210	0.8	44	25
5	170	840,106	I	24,575	227	0.8	39	250
6	1,152	6,550,187	I	52,881	489	0.8	41	1,500
7	5	8,066	I	6,278	58	0.8	42	25
8	27	99,994	I	21,403	198	0.8	28	37.5
9	21	68,847	I	27,140	251	0.8	43	37.5
10	76	350,279	R	114,103	573	0.9	2	100
11	420	1,585,376	R	308,880	1,552	0.9	54	500
12	91	423,972	R	128,665	647	0.9	4	150
13	55	259,589	R	60,870	306	0.9	6	75
14	146	676,063	R	201,141	1,011	0.9	30	200
15	6	24,338	R	1,719	9	0.9	18	25
16	138	655,735	R	159,390	801	0.9	22	200
17	90	449,899	R	121,954	613	0.9	8	150
18	10	48,347	R	11,620	58	0.9	31	25
19	81	374,790	R	88,777	446	0.9	16	100
20	24	98,388	C	16,109	149	0.85	29	37.5
21	24	35,067	C	3,987	37	0.85	34	37.5
22	9	12,180	C	1,624	15	0.85	27	25
23	49	56,530	C	4,867	45	0.85	35	75
24	30	36,350	C	5,441	50	0.85	14	37.5
25	74	109,745	C	11,990	111	0.85	38	100
26	35	47,181	C	4,419	41	0.85	10	50
27	79	120,429	C	15,379	142	0.85	33	100
28	108	143,182	C	36,866	341	0.85	12	150
29	779	1,655,836	C	155,232	1,436	0.85	36	1,000
30	9	12,288	C	1,572	15	0.85	26	25
31	20	38,001	C	6,691	62	0.85	11	25

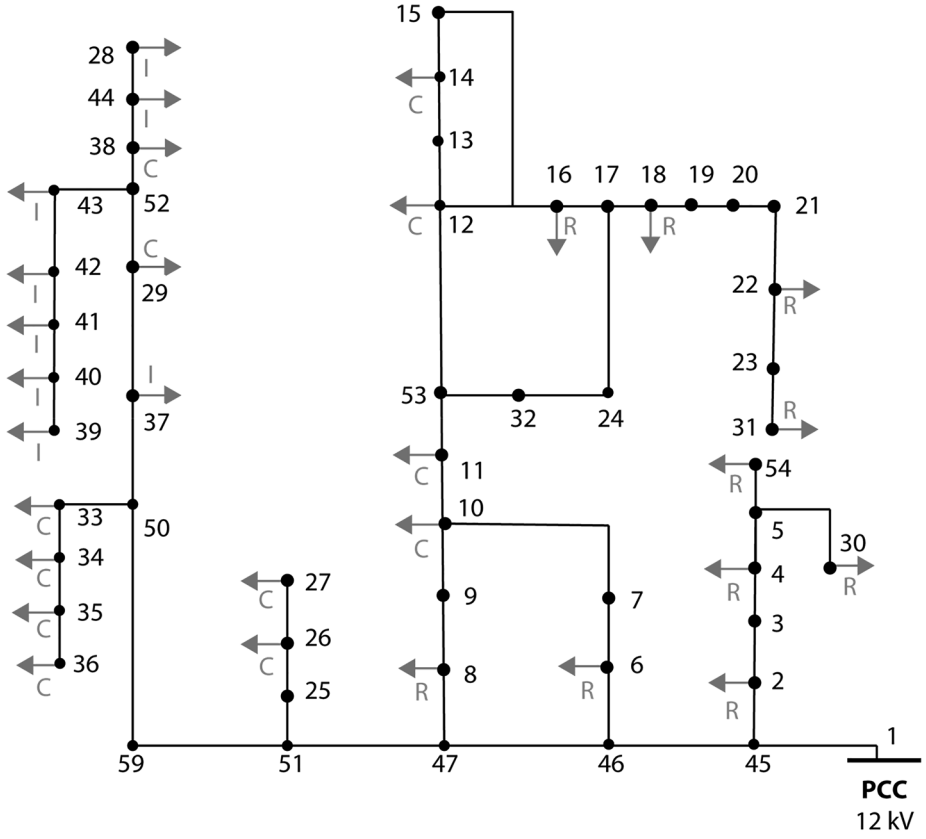

Fig. 5. Advanced Energy Community Low Voltage distribution grid network topology and load allocation (loads identified as residential, R, commercial, C, or industrial, I).

commercial properties. The power distribution system to support the community is a three-phase 12 kV feeder, which branches into single-phase, 240 V phase-to-phase (120 V phase-to-ground) circuits, for residential service and three-phase 480/277 V for commercial and industrial service.

The test system is comprised of 54 nodes, 56 branches, 31 clustered building loads, and 30 transformers. The Slack bus is node 1, and it represents the Point of Common Coupling (PCC) with the wide-area grid.

A load allocation was performed, using 31 representative buildings (and aggregated residential buildings), placing them in the nodes as shown in Fig. 5 and scaling up their loads (clustering) to obtain a representative share of loads from each sector. For this community, electricity demand is 60% Industrial, 27% Residential and 13% Commercial. The distribution transformer kVA ratings, listed in Table 3 were sized to accommodate the aggregated loads served (*i.e.*, all power flows kept below 1.p.u. loading), taking into consideration the discretized ratings of transformers that are commercially available. We assume only rooftop PV is installed in the community.

3.3. Cost and operational assumptions

All DER cost and operational assumptions used in this study are listed in Table 4. Our assumed capital cost for a battery storage system is based on the 2018 Lazard's Levelized Cost of Storage Analysis report [49], and it is specific to Lithium-ion, behind-the-meter Commercial & Industrial projects with battery storage co-located with PV. Also, the cost is composed of the storage module, the balance of system, and related engineering procurement and construction costs. We also assume that the O&M fixed cost is embedded in the capital cost monthly payments, and the variable O&M costs are assumed from [18].

DERopt also captures electrical utility rates for all building and sector types and also captures the intricacies of exporting electricity, under NEM and wholesale rates. Under NEM rates, the utility customer can export electricity at the rate at which it is purchased, or retail rates, minus a non-bypassable charge (typically around $0.02 per kWh). However, a utility customer can only export as much electricity as it is imported under NEM rates. Moreover, the customer can only receive credits on their monthly bill, and cannot receive direct payment. In DERopt, if more electricity is exported than imported, the excess is not credited to the utility customer under NEM rates, but the customer is still able to sell electricity under wholesale rates, with values that are typically around $0.02 per kWh.

The utility electricity tariffs modeled in DERopt are based on Southern California Edison Time-of-Use (TOU) rates schedules as of 2018. For large C&I customers, Schedule TOU-8-B-2 kV to 50 kV for

Table 4
DERopt Cost and Operational Assumptions.

Assumption	PV	EES
Capital Cost	2,000 $/kW (installed) [50]	600 $/kWh (installed) [49]
O&M Cost	0.001 $/kWh (generated) [18]	0.001 $/kWh (charged/discharged) [18]
Min SOC	–	0.1
Max SOC	–	0.95
Ramp rate	–	0.25 (% of capacity)
Efficiency	20%	90% (Charge/Discharge)
State of charge holdover	–	99.5%
Interest rate	8%	
Project lifetime	10 years	
Equity	20%	
Required Return	12%	

general service is adopted and for residential customers, Schedule TOU-D-A for domestic service is adopted. Fig. 6 illustrates the TOU rate schedules energy price ($/kWh) on the primary axis and demand charge ($/kW) on the secondary axis. Note that utility rates vary by season: Summer (from June to September, spanning 4 months) and Winter (from October to May, spanning 8 months) and also by day of the week (weekend versus weekday); for a given season and customer class, weekday rates are almost always more expensive than weekend rates. Moreover, in the TOU rate schedule assumed here, electricity prices can differ by up to nine-fold, which is the case for residential summer weekday on-peak rate versus off-peak rate. Demand charges are applied only to C&I customers and are also time-dependent. The differences in electricity price, driven by the TOU rate schedules, and demand charges strongly influence battery storage dispatch.

4. Results and discussion

The optimization algorithm is implemented in MATLAB R2015a [51] using the YALMIP R20181012 toolbox [52,53] and CPLEX v.12.8 [54] for the MILP solver. The k-medoids methodology reduces our dataset to 36 representative days for simulating the entire year; therefore, 864 hourly intervals are simulated. The hardware used for the optimization is an Intel Xenon CPU E5-2680 v2, 2.80 GHz server with 20 cores, 40 threads, and 32 GB of RAM. Simulation times average 280 s (with area and polygon transformer constraints, and around 41 min with island constraints. It is worth noting that piecewise linearization of the transformer constraints was implemented for the same scenarios and run times ranged from 25 to 30 min. Thus, polygon constraints are approximately 6 times faster.

The results presented in this section aim to identify the relevance and impacts of including transformer constraints (TC) in the design of AEC systems. To capture common district system and microgrid goals, two strategies are tested: (1) Zero Net Energy constrained, *i.e.*, to annually produce as much electricity as demanded, and (2) Islanding constraint, *i.e.*, to be able to meet critical loads under a non-planned utility grid network outage situation. The solar PV area constraint was also evaluated. Thus, the first set of scenarios simulated refer to ZNE operation with and without transformer constraints, the second set explores area constraints added to the first scenario set, and the third set employs the same constraints of the second set but explores a microgrid islanded operation instead of ZNE operation. The list of all scenarios simulated is given below:

1. **ZNE/ZNE + Transformer Constraints**: ZNE operation, constrained area for rooftop PV adoption, with or without transformer constraints;
2. **ZNE + Area Constraints/ZNE + Area Constraints + Transformer Constraints**: ZNE operation, constrained area for rooftop PV adoption, with or without transformer constraints;
3. **Island/ Island + Transformer Constraints:** Island operation, constrained area, with or without transformer constraint. It is assumed that critical loads are industrial and school, all other loads are shed. During islanding, there is no revenue for NEM and wholesale exports.

4.1. Using optimization to quantify and eliminate transformer overloads

In all scenarios, excessive amounts of PV power (or REES discharge in some cases) export are the root cause for transformer overload. The degree to which these overloads exceed transformer ratings (without transformer constraints considered) is shown in the left panels of Fig. 7, where each data point represents a transformer rated power capacity is plotted against its all-time maximum overload, *i.e.,* its maximum power injection recorded over the optimization timeframe. The x-axis was split into two data ranges: 25–500 kVA and 500–1500 kVA for better visualization of results. Overloaded transformers are shown in red and above the dotted line.

Out of a total of 31 transformers, the number of overloaded transformers was 13 for the first scenario, 17 for the second scenario, and 15 for the islanded scenario. The increase in transformer overloads when constraining the area points to the leveraging of the available physical area for PV deployment within the community, and the resulting increased PV adoption behind transformers feeding buildings with a larger rooftop area, namely transformers T11, T12, T29, T33, and T36. For almost all of those transformers, the maximum, area-constrained PV deployment is adopted (see Table 3 for maximum area-constrained PV deployment size and Table 6, in the Appendix, for transformer PV adoption) and these capacities lead to power production that is well beyond the transformer power ratings.

After transformer constraints are applied, the kVA flows through each transformer are forced to comply with their kVA power rating, and overloads are eliminated as shown in the right panels of Fig. 7. All transformer overloads were eliminated by either reducing PV adoption, increasing battery energy storage adoption, or curtailing PV at the C&I buildings.

Fig. 8 plots the net power flow through one given transformer, namely T54, over the optimization timeframe, before and after transformer constraints were applied; positive flows indicate exports to the grid. T54 is rated at 500 kVA and feeds a large residential load cluster and hosts a large PV adoption that is in the MW order of magnitude (we refer the reader to Table 6 in the appendix for the detailed adoption values for all scenarios). Overloads, which occurred in the scenario without transformer constraints, are indicated by the solid red curve and are compared against the transformer-constrained operation, indicated by the dashed blue curve. Notice that high exports of excess PV generation cause overloads. These high exports, however, are removed in the constrained scenarios through the adoption of battery energy storage, which “clips” the high PV exports by charging with the excess PV generation. Transformer constraints leveraged the adoption of 855 kWh of combined EES and REES for the ZNE case. For the area-constrained ZNE case, this adoption is even higher, at 2332 kWh, to meet ZNE with a reduced PV adoption.

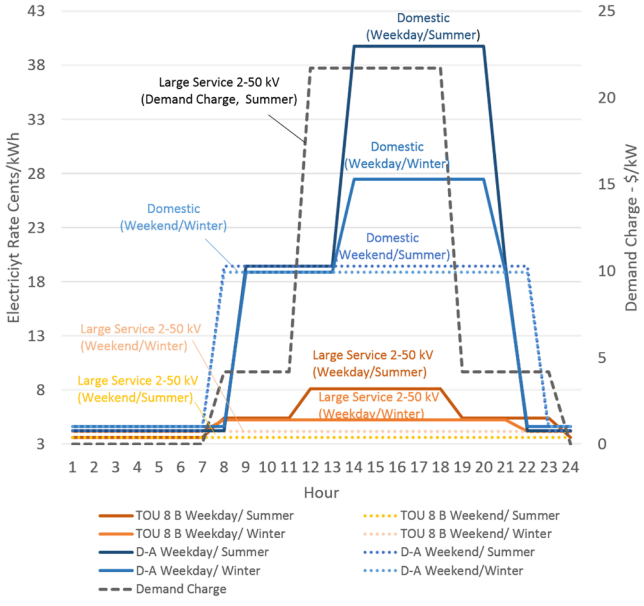

Fig. 6. Rate structures for utility electricity. Schedule TOU-8-B is used for large C&I utility customers, and Schedule D-A is used for residential utility customers. Color shows detail on different Schedules. Weekend rates are shown by dotted lines, and the secondary axis shows demand rates on dashed lines.

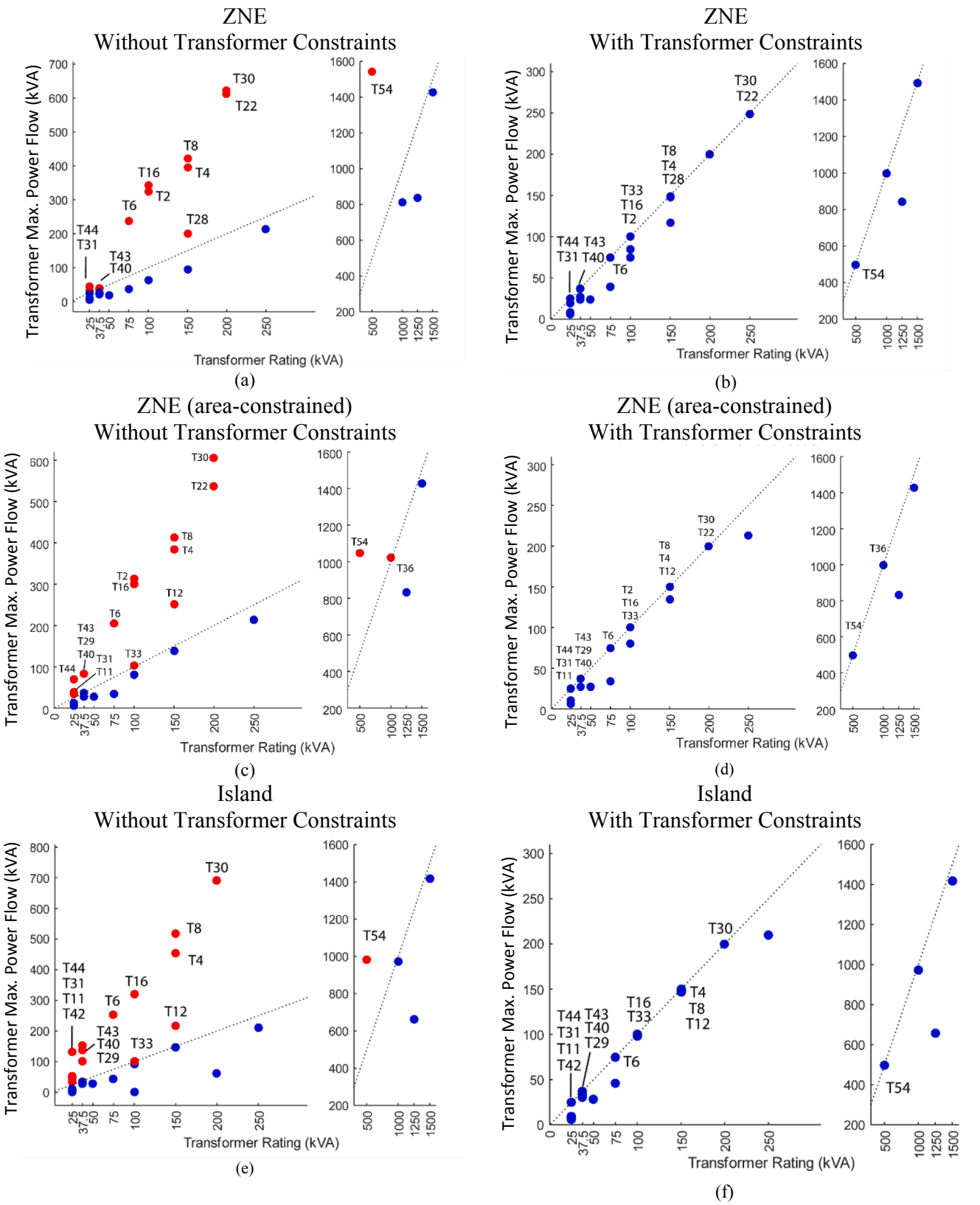

Fig. 7. Transformer overloads for (a) ZNE without transformer constraints and (b) ZNE with transformer constraints. (c) ZNE without transformer constraints and (d) ZNE with transformer constraints, (e) Island, without transformer constraints and (f) Island, with transformer constraints.

4.2. Impacts of transformer constraints on DER allocation

Fig. 9 compares the DER allocations in each individual building for each scenario set. Buildings 1–9 are industrial loads, buildings 9–19 are residential loads and buildings 20–31 are commercial loads. The first scenario set (Fig. 9a) does not impose any constraints on the area available for PV installation. With no transformer constraints applied, PV is adopted in proportion to the magnitude of the building loads.

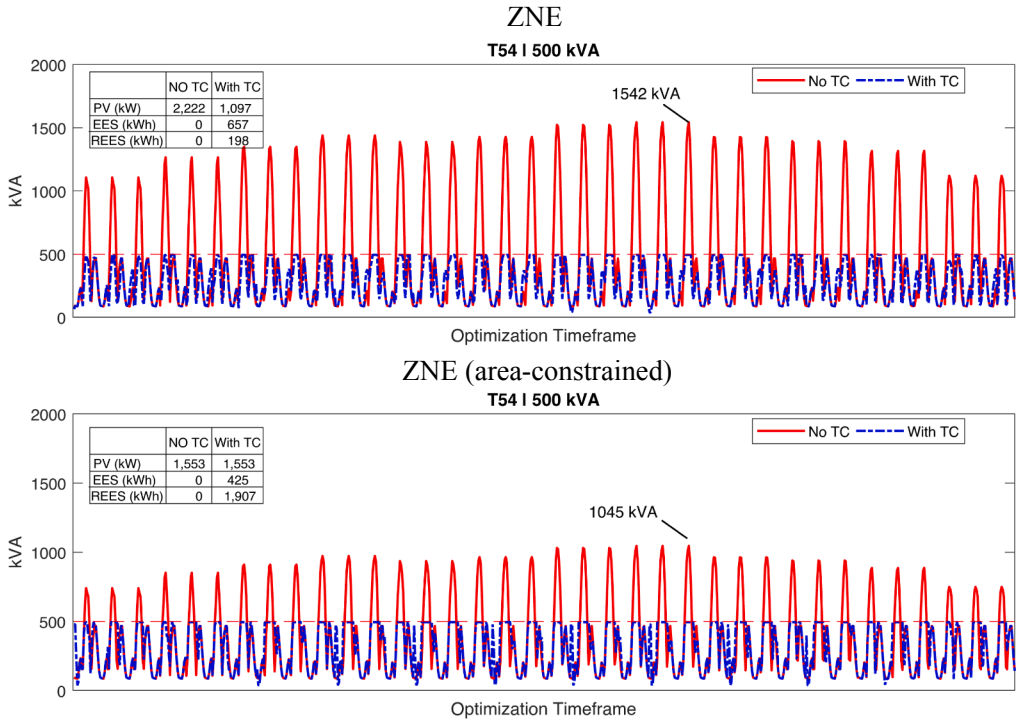

Fig. 8. Transformer 54 (500 kVA) kVA power flows: comparison of before (solid red curve) and after (blue dashed curve) transformer constraints for ZNE (top), ZNE area-constrained (middle) and island (bottom) scenarios.

Therefore, most (63%, or 6.7 MW) of the total community PV capacity is adopted in the residential sector, as our test case has a large number of residential loads, followed by the industrial sector (24%, or 2.53 MW), and commercial sector (13%, or 1.37 MW). This allocation, overloads local transformers, as shown in Fig. 7. When transformer constraints are added, however, the PV capacity is redistributed leading to a shift of the PV capacity from the residential to the C&I sector, which has its typically larger transformer capacity leveraged to compensate for the reduction in PV on the residential sites, with smaller transformers. For instance, the PV adoption is reduced at Building 11, a cluster of residential buildings (from 2222 kW to 1096 kW) and increased at Building 6, an industrial site (from 894 to 2766 kW).

After imposing area constraints for PV installation (Fig. 9b), PV adoption becomes more evenly distributed across the buildings in the community, and little to no EES/REES is adopted. Intuitively, area constraints recommend PV system placement not at the buildings with larger loads but upon the buildings with available rooftop space. The constraint leverages the buildings in the residential and commercial sectors with enough area available for PV adoption to support the demand in the industrial sector, which cannot meet the energy demand using onsite PV. As discussed previously, this is often true for industrial building types, and regarding our test-case system, this fact is illustrated in Fig. 4. Thus, these loads will likely depend upon energy imports from neighboring buildings, which reinforces the benefits of aggregating various loads as a community/microgrid if the goal is community-scale ZNE. As a result, the PV adoption in the vast majority of commercial and residential buildings equals to the maximum amount of area-limited maximum PV hosting capacity. For instance, PV adoption on Building 36, a cluster of commercial loads, is increased from 876 kW to 1,436 kW, the local area-constrained maximum PV capacity. This DER allocation, however, causes overloads, especially in residential transformers that are typically smaller in power capacity. When transformer constraints are added, transformer overloads are avoided through the adoption of EES/REES. REES storage is shown to be preferred (Fig. 9) since discharge for grid export is allowed.

For the island case, a significant amount of storage is deployed to accomplish islanding even without transformer constraints. Nonetheless, excessive exports to meet neighboring loads also cause transformer overloads. Therefore, there is a shift from EES to REES investment since batteries are extensively required to export to neighbors.

In sum, all previous cases highlight the value of an optimal DER investment planning with transformer constraints, especially in area-constrained situations, where the local PV capacity must be high and can't be reduced to meet ZNE goals, and storage must be deployed to avoid transformer overloads. The optimization can find the least cost allocation, where and how much DER should be installed, even though it might not have been the most obvious solution employing other commonly used grid constraints such as bus voltage and line ampacity limits.

From the aggregate AEC perspective, for all scenarios, transformer constraints promote a slight increase in overall PV adoption, which is always accompanied by an increase in battery energy storage adoption. Table 5 lists the total DER adoption per DER type (PV, EES, and REES) for each scenario, where the trend described above is confirmed. At first, the increase in total PV adoption with transformer constraints may seem counterintuitive. We suspect that this increase is driven by the round-trip efficiency (RTE) of battery energy storage. A case run with 100% RTE for both EES and REES shows a marginal 1.4% increase in PV adoption, which confirms our guess. Moreover, from a design perspective, this trend is indeed reasonable, since the increased PV and battery storage capacity is (1) better sized to meet loads locally while avoiding large imports and exports that will result in transformer overloads, and (2) more distributed amongst buildings, as shown in Fig. 9.

In total, for the area-unconstrained ZNE case transformer constraints add 101 kW of PV (1% increase), 2,104 kWh of EES (6 fold increase) and 254 kWh of REES (inexistent beforehand). For the area-constrained ZNE case, transformer constraints add 631 kW of PV (5.6% increase), 2,259 kWh of EES (12 fold increase), and 10,844 kWh of REES (inexistent beforehand). For the islanded case, transformer constraints do not significantly change the total PV and EES plus REES

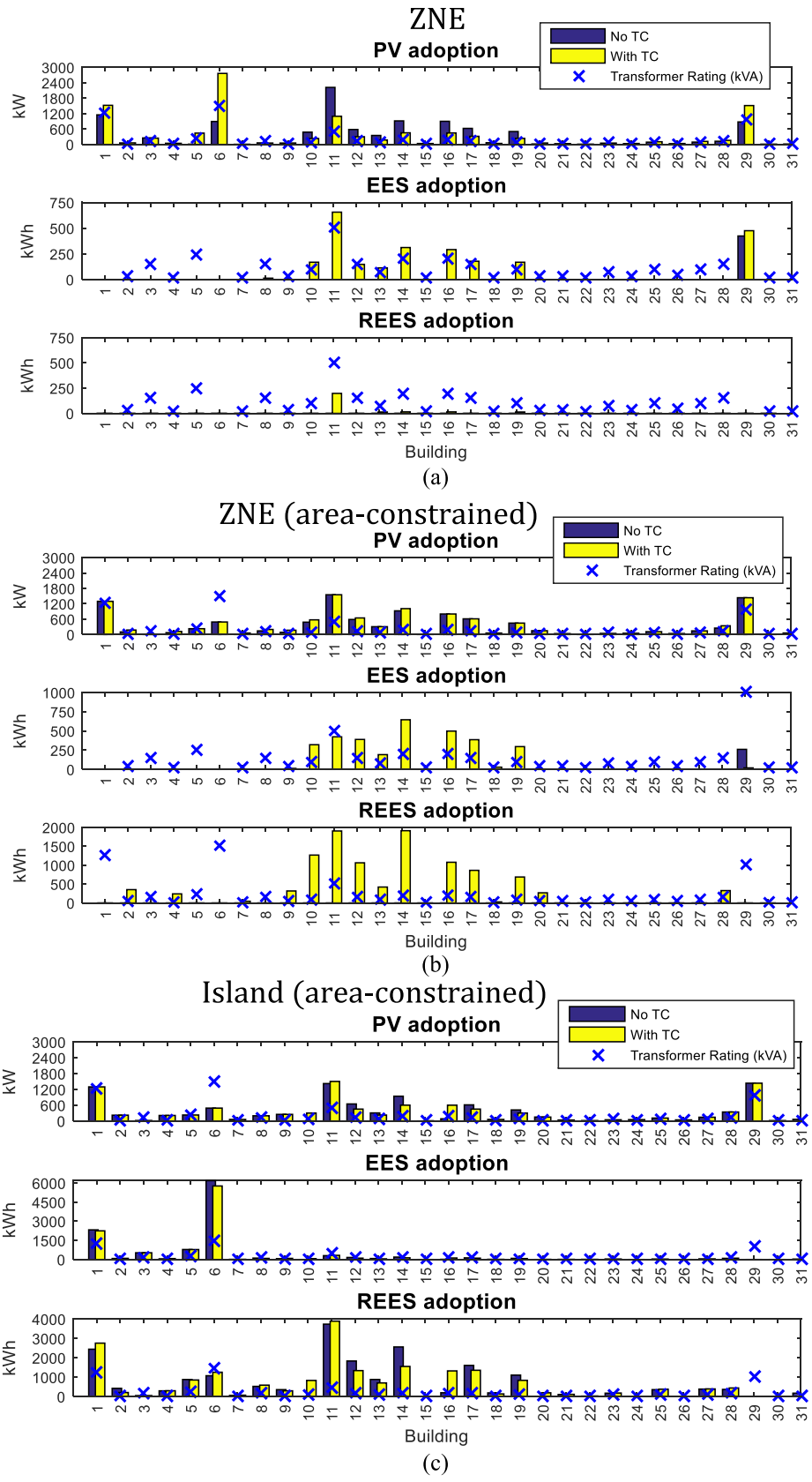

Fig. 9. Building DER allocation comparison with and without transformer constraints for scenarios: (a) ZNE, (b) ZNE (area-constrained), and (c) Island (area-constrained). Transformer kVA ratings are indicated by an x marker. Table 6 in the appendix provides a list of all DER allocation at all individual buildings for all scenarios.

Table 5
Total Building DER adoption for all scenarios.

Scenario	DER Type	Total DER allocated	
		Without Transformer Constraints	With Transformer Constraints
ZNE (unconstrained)	**PV (kW)**	10,585	10,686
	EES (kWh)	424	2,528
	REES (kWh)	0	254
ZNE (area-constrained)	**PV (kW)**	10,580	11,211
	EES (kWh)	261	3,220
	REES (kWh)	0	10,844
Island (area-constrained)	**PV (kW)**	9,902	9,914
	EES (kWh)	11,402	10,976
	REES (kWh)	19,875	20,280

combined installed capacity; interestingly, PV and total storage capacities remain identical for practical purposes (ignoring differences below 10 kW/20 kWh). However, the locations of the DER resources change noticeably: the optimization reduces PV adoption in certain buildings, to remove transformer overloads while relocating storage (both EES and REES), and migrating 426 kWh of EES storage capacity to REES.

The different DER allocations of Table 5 produce different total project costs. For the ZNE scenarios, adding transformer constraints substantially increased cost. For our specific test case, the first year of operation total cost (including equipment capital cost and operational costs) for the ZNE scenario with no transformer constraints is about $3.5 million. When transformer constraints are added, this cost goes up to $3.81 million. Similarly, for the area-constrained ZNE case, the first-year cost is $3.57 million without transformer constraints and $5.07 million with transformer constraints. The need for battery energy storage adoption drives the cost increase. However, for the island scenario, since the initial storage adoption was already required for islanding, there is not a significant difference between costs before and after transformer constraints are applied; the total cost is $6.66 million without transformer constraints and $6.67 million with transformer constraints

4.3. Transformer versus storage investment costs

To address the choice of installing storage instead of upgrading transformer infrastructure, we provide a brief analysis of costs for each option. In total, using the cost assumptions from Table 4, the annual electricity costs for the Oak View AEC ZNE scenario increase by over $1.5 million (this includes the annual amortized capital cost and also operation costs/revenue over one year). However, a simple cost exercise might show the value of adding this extra DER capacity. First, the total additional transformer capacity that would otherwise be needed to accommodate the PV reverse power flows to achieve community ZNE is 6,565 kVA. Assuming a transformer replacement cost of $147/kVA [55], the total cost of all replacements would be $965,055. However, with additional DER, the amount of revenue per kWh exported at the PCC increases from (from $0.17 to $0.26 per kWh). This happens because battery storage reduces grid imports (and in turn exports because of ZNE operation) at the PCC in 48% (from 8.58 GWh to 4.49 GWh). Simultaneously, REES performs arbitrage, that is, delayed export until peak cost periods. All of these effects and capabilities could become extremely valuable to the utility grid network that attempts to support very high renewable penetrations. The added flexibility inherent to battery storage will likely introduce possibilities for new and more valuable revenue streams, not yet considered in this study, building the case for a possible recovery of the investment throughout the project lifetime.

Additionally, with the added storage, the PV electricity used to directly power the AEC loads increases by 12%. Moreover, the reduced grid imports avoid a total of 7,040 $MTCO_2$ over 10 years, estimated considering the hourly grid emission factors for the CAISO grid in 2018 [56]. Moreover, before any DER deployment, 17.39 GWh is imported from the grid to meet the annual AEC demand. After PV and battery storage deployments, at best, the total grid electricity imports are reduced by 74% (to 4.49 GWh), and 5.94 GWh electricity is exported at the PCC back to the bulk system (due to the ZNE constraint) as renewable PV electricity. The total carbon emissions offset would consider both the time-resolved offset associated with utility imports and the marginal carbon benefit of exporting excess renewable generation back to the utility. The detailed analysis required to resolve a useful approximation of these emissions currently falls outside the scope of this work.

From a technical perspective, locally deploying storage to prevent transformer overloads avoids extremely high reverse power flows, which guarantees that the “duck curve” effect [57] does not propagate upstream in the distribution system which would require infrastructure upgrades elsewhere. Extending this problem to include additional adjacent communities, the connecting electrical infrastructure, and decisions surrounding infrastructure upgrades and community versus utility energy resources would begin to capture the various tradeoffs that must be considered as society moves to high renewable penetration. Moreover, the current analysis does not capture the cost benefits from the added resilience and reliability inherent to the local generation and storage. Lastly, as is shown for the islanding scenario when storage is inevitably necessary, transformer constraints will provide valuable information on where to locate these assets, while the sole use of line and voltage constraints may not.

5. Summary and conclusions

This work developed a mixed integer linear program for the optimal DER investment planning and operation of an advanced energy community microgrid, constrained by available physical space for rooftop solar PV deployment and also grid constraints with a novel technique to include transformer power constraints. We used a real-world test case, involving 31 customer loads modeled in EnergyPlus, to accurately represent the community aggregated load stock of residential, commercial, and industrial utility customers. We modeled operation goals typically desired for district systems such as Zero-Net-Energy and islanding as a microgrid during unplanned grid outages.

Regarding DER allocation in urban district systems, in order to meet ZNE or islanding goals within an AEC, our results show that:

- **In urban district systems, ZNE can only be accomplished at a community level;** large utility customers in the C&I sector most likely cannot entirely deploy enough PV to meet local electricity demand since they typically have high demand and there is a limited amount of space available for rooftop PV deployment at those sites.

Therefore, to accomplish ZNE, the available area for PV installation in the residential sector needs to be leveraged to support the community energy goals.

- **Transformer overloads will likely occur as a result of high PV deployments in low voltage urban networks due to transformer sizes that were not designed to consider significant reverse power flow of PV electricity. Thus, including transformer constraints in the optimization problem formulation will provide a more accurate DER allocation;** the large amount of local solar PV required to meet ZNE is most times larger than what currently installed low-voltage utility distribution transformers can handle. Thus, the negative grid impacts associated with a high PV penetration will not only manifest as voltage and line ampacity margins being violated, which is the main focus of previous literature but also likely be accompanied by transformer overloads due to high reverse power flows (excess PV exported back to the grid).
- **It is possible to altogether remove transformer overloads while integrating high penetrations of solar PV into the AEC without any required transformer upgrades;** integrating transformer constraints into a MILP optimization to limit the power flows at the transformer level produces entirely different optimal DER allocation and operation results. The main strategies to avoid overloads are deploying battery energy storage and also optimally re-distributing PV throughout the community.
- **Polygon relaxations are a practical linearization approach for transformer power flow constraints;** using polygon relaxations to capture the non-linear relationship between active and reactive power flows at the transformer showed adequate accuracy (errors below 1%), and computation tractability (run times of approximately 4 min), as well as superior computational performance. When compared to comparable linearization methods such as piecewise linearization or linear interpolation, polygon relaxation run time is about six times faster.
- **The use of transformer constraints within DER investment planning, associated with the right BESS allocation and dispatch, will effectively increase PV penetration as opposed to the use of practical rules, such as the "15%" rule.** Taking the ZNE, area-constrained scenario as an example, the total PV installed capacity over the entire community is 11,211 kW which is 1.7 times greater than the total installed transformer capacity of 6,500 kVA, and about 10 times the AEC peak load of 1,143 kW, which shows an excellent potential for PV hosting capacity maximization beyond conservative rules of thumb.

In light of our model limitations, future work involves, modifying the model to include the impact of other, new and emerging, energy generation technologies. Future work also includes implementing a full decoupled, linearized power flow solution suitable for meshed microgrids, namely the Decoupled Linearized Power Flow [58] into the formulation to explicitly model other grid constraints such as voltage and branch ampacity.

Acknowledgements

The authors gratefully acknowledge the financial support for this work, which was provided by the California Energy Commission, contract number: EPC-15-077, and the significant leadership and contributions of Rachel Salazar, our Contract Manager.

Appendix A. Building DER allocation

Table 6
Building DER allocation for all scenarios.

#	ZNE			ZNE + TC			ZNE + area			ZNE + area + TC			Island + area			Island + area + TC		
BDG	PV	EES	REES	PV	EES	REES	PV	EES	REES	PV	EES	REES	PV	EES	REES	PV	EES	REES
1	1152	0	0	1523	0	0	1296	0	0	1296	0	0	1296	2328	2445	1296	2250	2758
2	58	0	0	61	0	0	101	0	0	175	0	354	221	79	428	221	92	211
3	253	0	0	245	0	0	18	0	0	18	0	0	18	528	55	18	528	55
4	45	0	0	43	0	0	73	0	0	120	0	241	210	54	298	210	72	302
5	11	0	0	442	0	0	227	0	0	227	0	0	227	784	883	227	780	857
6	894	0	0	2766	0	0	489	0	0	489	0	0	489	6191	1077	489	5774	1258
7	5	0	0	7	0	0	13	0	0	58	0	46	58	13	62	58	15	73
8	60	0	0	54	13	0	142	0	0	198	0	0	198	109	528	198	86	591
9	54	0	0	55	0	0	88	0	0	168	13	319	251	66	360	251	87	299
10	478	0	0	230	169	0	482	0	0	573	321	1268	0	0	0	301	67	835
11	2222	0	0	1096	656	198	1552	0	0	1552	424	1907	1422	302	3736	1503	324	3892
12	582	0	0	299	148	0	588	0	0	647	390	1064	647	159	1837	451	104	1343
13	350	0	0	172	114	13	306	0	0	306	192	422	306	76	885	225	53	706
14	917	0	0	453	312	15	925	0	0	1011	646	1914	942	188	2562	601	132	1556
15	36	0	0	36	0	0	9	0	0	9	0	0	0	0	0	9	0	0
16	901	0	0	446	292	15	801	0	0	801	499	1078	83	15	199	601	118	1327
17	625	0	0	316	178	0	613	0	0	613	387	864	613	128	1612	451	105	1359
18	66	0	0	39	0	0	58	0	0	58	29	28	58	16	192	58	13	139
19	502	0	0	236	169	13	446	0	0	446	297	688	420	88	1109	301	72	840
20	17	0	0	56	0	0	149	0	0	149	0	270	149	0	0	149	13	197
21	29	0	0	33	0	0	37	0	0	37	0	0	37	13	109	37	13	117
22	10	0	0	12	0	0	15	0	0	15	0	0	15	13	27	15	13	33
23	49	0	0	52	0	0	45	0	0	45	0	0	45	40	177	45	38	185
24	31	0	0	37	0	0	50	0	0	50	0	0	50	0	0	50	0	0
25	89	0	0	104	0	0	111	0	0	111	0	0	111	37	359	111	35	382
26	29	0	0	36	0	0	41	0	0	41	0	0	41	0	0	41	0	0
27	90	0	0	118	0	0	142	0	0	142	0	0	142	51	388	142	49	396
28	124	0	0	159	0	0	251	0	0	341	0	329	341	89	372	341	101	446
29	876	424	0	1515	476	0	1436	261	0	1436	20	0	1436	0	0	1436	0	0
30	10	0	0	12	0	0	15	0	0	15	0	0	15	0	0	15	0	0
31	17	0	0	34	0	0	59	0	0	62	0	51	62	34	176	62	41	125
Total	10585	424	0	10686	2528	254	10580	261	0	11211	3220	10844	9902	11402	19875	9914	10976	20280

References

[1] Jahangiri P, Aliprantis DC. Distributed Volt/VAr control by PV inverters. IEEE Trans Power Syst 2013;28:3429–39.
[2] von Appen J, Braun M, Stetz T, Diwold K, Geibel D. Time in the sun: the challenge of high PV penetration in the german electric grid. IEEE Power Energ Mag 2013;55–64. https://doi.org/10.1109/MPE.2012.2234407.
[3] Prakash P, Khatod DK. Optimal sizing and siting techniques for distributed generation in distribution systems: a review. Renew Sustain Energy Rev 2016;57:111–30.
[4] Electric Power Research Institute (EPRI). An overview of advanced energy communities; 2017.
[5] Electric Power Research Institute (EPRI). Grid integration of zero net energy communities - final report. 2021; 2016.
[6] Electric Power Research Institute (EPRI). Alternatives to the 15% rule: modeling and hosting capacity analysis of 16 feeders; 2015.
[7] Palmintier B, et al. On the path to SunShot: emerging issues and challenges in integrating solar with the distribution system; 2016. doi:NREL/TP-5D00-6533, SAND2016-2524.
[8] Ismael SM, Abdel Aleem SHE, Abdelaziz AY, Zobaa AF. State-of-the-art of hosting capacity in modern power systems with distributed generation. Renew Energy 2019;130:1002–20.
[9] Southern California Edison (SCE). Distributed energy resource interconnection map (DERiM); 2016.
[10] Rezaee Jordehi A. Allocation of distributed generation units in electric power systems: a review. Renew Sustain Energy Rev 2016;56:893–905.
[11] Arabali A, Ghofrani M, Bassett JB, Pham M, Moeini-Aghtaei M. Chapter 7 - Optimum sizing and siting of renewable-energy-based DG units in distribution systems. Optimization in renewable energy systems Elsevier Ltd; 2017. https://doi.org/10.1016/B978-0-08-101041-9.00007-7.
[12] Conforti M, Cornuéjols G, Zambelli G. Integer programming. Springer; 2014. doi:10.1007/978-3-319-11008-0.
[13] Mansini R, Ogryczak W, Speranza MG. Linear and mixed integer programming for portfolio optimization. Linear and Mixed Integer Programming for Portfolio Optimization; 2015. doi:10.1007/978-3-319-18482-1.
[14] Ren H, Gao W. A MILP model for integrated plan and evaluation of distributed energy systems. Appl Energy 2010;87:1001–14.
[15] Ren H, Zhou W, Nakagami K, Gao W, Wu Q. Multi-objective optimization for the operation of distributed energy systems considering economic and environmental aspects. Appl Energy 2010;87:3642–51.
[16] Stadler M, Groissböck M, Cardoso G, Marnay C. Optimizing Distributed Energy Resources and building retrofits with the strategic DER-CAModel. Appl Energy 2014;132:557–67.
[17] Falke T, Krengel S, Meinerzhagen A-K, Schnettler A. Multi-objective optimization and simulation model for the design of distributed energy systems. Appl Energy 2016;184:1508–16.
[18] Flores RJ, Brouwer J. Optimal design of a distributed energy resource system that economically reduces carbon emissions. Appl Energy 2018;232:119–38.
[19] Huang W, Zhang N, Yang J, Wang Y, Kang C. Optimal configuration planning of multi-energy systems considering distributed renewable energy. IEEE Trans Smart Grid 2017;3053:1–12.
[20] Basu AK, Bhattacharya A, Chowdhury S, Chowdhury SP. Planned scheduling for economic power sharing in a CHP-based micro-grid. IEEE Trans Power Syst 2012;27:30–8.
[21] Morvaj B, Evins R, Carmeliet J. Optimization framework for distributed energy systems with integrated electrical grid constraints. Appl Energy 2016;171:296–313.
[22] Yang Y, Zhang S, Xiao Y. Optimal design of distributed energy resource systems coupled with energy distribution networks. Energy 2015;85:433–48.
[23] Yang Y, Zhang S, Xiao Y. An MILP (mixed integer linear programming) model for optimal design of district-scale distributed energy resource systems. Energy 2015;90:1901–15.
[24] Mashayekh S, et al. Security-constrained design of isolated multi-energy microgrids. IEEE Trans Power Syst 2017. https://doi.org/10.1109/TPWRS.2017.2748060.
[25] Qiu J, Zhao J, Yang H, Wang D, Dong ZY. Planning of solar photovoltaics, battery energy storage system and gas micro turbine for coupled micro energy grids. Appl Energy 2018;219:361–9.
[26] Grover-Silva E, Girard R, Kariniotakis G. Optimal sizing and placement of distribution grid connected battery systems through an SOCP optimal power flow algorithm. Appl Energy 2018;219:385–93.
[27] Wang Z, Chen B, Wang J, Kim J, Begovic MM. Robust optimization based optimal DG placement in microgrids. IEEE Trans Smart Grid 2014;5:2173–82.
[28] Grover-Silva E, et al. A stochastic optimal power flow for scheduling flexible resources in microgrids operation. Appl Energy 2018;229:201–8.
[29] Santos SF, Fitiwi DZ, Shafie-khah M, Bizuayehu AW, Catalão JPS. Optimal sizing and placement of smart-grid-enabling technologies for maximizing renewable integration. Smart Energy Grid Eng 2016. https://doi.org/10.1016/B978-0-12-805343-0.00003-6.
[30] Chanda S, De A. A multi-objective solution algorithm for optimum utilization of Smart Grid infrastructure towards social welfare. Int J Electr Power Energy Syst 2014;58:307–18.
[31] Flores R, Brouwer J. Optimal design of a distributed energy resources system that minimizes cost while reducing carbon emissions. ASME 2017 11th international conference on energy sustainability. 2017.
[32] Li B, Roche R, Paire D, Miraoui A. Sizing of a stand-alone microgrid considering electric power, cooling/heating, hydrogen loads and hydrogen storage degradation. Appl Energy 2017;205:1244–59.
[33] Mashayekh S, Stadler M, Cardoso G, Heleno M. A mixed integer linear programming approach for optimal DER portfolio, sizing, and placement in multi-energy microgrids. Appl Energy 2016;187:154–68.
[34] Ehsan A, Yang Q. Scenario-based investment planning of isolated multi-energy microgrids considering electricity, heating and cooling demand. Appl Energy 2019;235:1277–88.
[35] Alturki M, Khodaei A, Paaso A, Bahramirad S. Optimization-based distribution grid hosting capacity calculations. Appl Energy 2018;219:350–60.
[36] Flores R, et al. Huntington beach advanced energy community blueprint; 2018.
[37] White D. Important factors for early market microgrids: demand response and plug-in electric vehicle charging. Irvine: Univeristy of California; 2016.
[38] Tesla. Powerwall Technical Specs; 2019. Available at: https://www.tesla.com/powerwall.
[39] Kurtz EB, Shoemaker TM, Mack JE. (Engineer). The lineman's and cableman's handbook. 18-8 through 18-15; 1997.
[40] U.S.Department of the Interior Bureau of Reclamation - Facilities Enineering Branch. Permissible Loading of Oil-Immersed Transformers and Regulators. 2000;1–5:1–25.
[41] Archimedes (ed.Heath). Works of Archimedes. Cambridge University Press; 1897.
[42] Erdal M. Optimal thrust allocation for dynamic positioning systems using linear programming and quadratic programming; 2015.
[43] Ahmadi H, Member S, Mart JR. Linear current flow equations with application to distribution systems reconfiguration. 2015;30:2073–80.
[44] Gholami A, Shekari T, Grijalva S. Proactive management of microgrids for resiliency enhancement: an adaptive robust approach. IEEE Trans Sustain Energy 2019;10:470–80.
[45] McDonald AN. Method for calibrating community scale energy demand using whole building simulation tools for advanced energy community planning; 2017.
[46] Domínguez-Muñoz F, Cejudo-López JM, Carrillo-Andrés A, Gallardo-Salazar M. Selection of typical demand days for CHP optimization. Energy Build 2011;43:3036–43.
[47] Southern California Edison. Schedule TOU-D TIME-OF-USE DOMESTIC; 2019.
[48] Folsom Labs. Helioscope [Software]; 2017.
[49] Lazard. Levelized Cost of Storage Analysis - version 4.0; 2018. doi:10.1097/01.psy.0000529859.93952.b1.
[50] Lazard. Lazard's Levelized Cost of Energy Analysis - version 12.0. 0–19; 2018.
[51] The MathWorks Inc. MATLAB v.2011a.
[52] Löfberg, J. YALMILP; 2019.
[53] Lofberg J. YALMIP : a toolbox for modeling and optimization in MATLAB. 2005:284–9. doi:10.1109/cacsd.2004.1393890.
[54] IBM. CPLEX; 2017.
[55] PG&E. Transformer unit cost data sheet received from utility distribution planner; 2016.
[56] CAISO. Greenhouse Gas Emission Tracking Report - Total hourly GHG emissions to serve ISO load; 2018. Available at: http://www.caiso.com/market/Pages/ReportsBulletins/RenewablesReporting.aspx#ghgreport%0A.
[57] California Independent System Operator (CAISO). What the duck curve tells us about managing a green grid; 2016. Available at: https://www.caiso.com/documents/flexibleresourceshelprenewables_fastfacts.pdf.
[58] Yang J, Zhang N, Kang C, Xia Q. A state-independent linear power flow model with accurate estimation of voltage magnitude. IEEE Trans Power Syst 2016;8950:1.